MUSIC-CSR: Hyperspectral Unmixing via Multiple Signal Classification and Collaborative Sparse Regression

Marian-Daniel Iordache, José M. Bioucas-Dias, *Member, IEEE*,
Antonio Plaza, *Senior Member, IEEE*, and Ben Somers

Abstract

Spectral unmixing aims at finding the spectrally pure constituent materials (also called *endmembers*) and their respective fractional abundances in each pixel of a hyperspectral image scene. In recent years, sparse unmixing has been widely used as a reliable spectral unmixing methodology. In this approach, the observed spectral vectors are expressed as linear combinations of spectral signatures assumed to be known *a priori* and present in a large collection, termed *spectral library* or *dictionary*, usually acquired in laboratory. Sparse unmixing has attracted much attention as it sidesteps two common limitations of classic spectral unmixing approaches: the lack of pure pixels in hyperspectral scenes and the need to estimate the number of endmembers in a given scene, which are very difficult tasks. However, the high mutual coherence of spectral libraries, jointly with their ever-growing dimensionality, strongly limits the operational applicability of sparse unmixing. In this paper, we introduce a two-step algorithm aimed at mitigating the aforementioned limitations. The algorithm exploits the usual low dimensionality of the hyperspectral data sets. The first step, similar to the *multiple signal classification* (MUSIC) array signal processing algorithm, identifies a subset of the library elements which contains the endmember signatures. Because this subset has cardinality much smaller than the initial number of library elements, the sparse regression we are led to is much more well-conditioned than the initial one using the complete library. The second step applies *collaborative sparse regression* (CSR), which is a form of structured sparse regression, exploiting the fact that only a few spectral signatures in the library are active. The effectiveness of the proposed approach, termed MUSIC-CSR, is extensively validated using both simulated and real hyperspectral data sets.

Index Terms

Hyperspectral imaging, hyperspectral unmixing, spectral libraries, sparse unmixing, sparse regression, collaborative sparse regression, dictionary pruning, MUSIC, array signal processing.

M.-D. Iordache and B. Somers are with the Flemish Institute for Technological Research (VITO), Centre for Remote Sensing and Earth Observation Processes (TAP), Boeretang 200, BE-2400 Mol, Belgium. J. M. Bioucas-Dias is with the Instituto de Telecomunicações and Instituto Superior Técnico, TULisbon, 1049–001, Lisbon, Portugal. A. Plaza is with the Hyperspectral Computing Laboratory, Department of Technology of Computers and Communications, Escuela Politécnica, University of Extremadura, Cáceres, E-10071, Spain.

I. Introduction

Spectral unmixing is an important technique for hyperspectral data exploitation [1]. It decomposes the (possibly mixed) pixel spectra measured by an imaging spectrometer into a collection of pure constituent spectra (called *endmembers*) and their corresponding fractional abundances, which quantify the proportion of each pure material in the pixel [2]. Mixed pixels appear due to the relative low spatial resolution of the sensor flying at high altitudes, or because the materials form intimate mixtures [3]. In a linear spectral unmixing scenario, the mixed pixels can be expressed as a linear combination of the endmember signatures present in the scene weighted by their respective fractional abundances. The exploitation of this model, in spite of its simplicity, has fostered a large amount of research leading to a plethora of endmember extraction and abundance estimation algorithms developed with (and without) the assumption that pure pixels[1] can be found in the original hyperspectral image. A detailed review of techniques developed for spectral unmixing in recent years is available at [4].

Linear spectral unmixing has been recently addressed under a sparse regression framework [5], [6]. The core assumption in this framework is that the observed (generally mixed) spectra measured by a hyperspectral imaging instrument is well approximated by a linear combination of a small (*i.e.,* sparse) subset of spectral signatures selected from a large (usually overcomplete) library. As shown in [4], this sparse unmixing formulation has attracted much attention, as it sidesteps two well known obstacles in classic spectral unmixing methods. First, sparse unmixing does not require the presence of pure signatures in the data, as the endmembers used for spectral mixture modeling are collected from a library of pure signatures. Second, sparse unmixing does not require the estimation of the number of endmembers in a given scene, which has been shown to be a challenging process in the literature.

The ability to obtain meaningful unmixing results by seeking sparse solutions of underdetermined linear systems of equations depends on the degree of sparseness of the mixtures[2] and on the coherence of the library signatures, measured *e.g.*, in terms of the so-called *mutual coherence* [7] or of the *restricted isometric constants* [8]. Qualitatively, the higher the *mutual coherence*, the lower the degree of sparseness ensuring perfect unmixing. Unfortunately, it happens that in hyperspectral applications the mutual coherence is often very high (*i.e.,* close to 1), thus, limiting the success of the unmixing via sparse regression. This drawback is somehow mitigated by the very high degree of sparseness (or low number of endmembers) that most hyperspectral applications exhibit. For an extensive study on these issues, see [5].

The aforementioned limitation has been partially mitigated by promoting some type of structured sparsity in the unmixed solutions via suitable regularization terms. Three relevant examples are the total variation (TV) spatial regularizer [9], which promotes piecewise-smooth fractional abundances, the group-based regularizer in [10], [11], which promotes pre-defined groups of active endmembers in a single fractional abundance vector, and the mixed norm regularizers, which promotes the same set of active endmembers across all fractional abundance vectors [12] (thus the name *collaborative* sparse regression (CSR)).

[1] A pure pixel contains just one endmember.

[2] *i.e.,* the number of library signatures with nonzero weights participating in the mixture.

A. Related work

Let us assume that the hyperspectral data set to be unmixed is well approximated by the linear mixing model. In this case, the objective of sparse regression is the determination of the unknown fractional abundance vectors that share a common sparse support. This is the so-called multiple measurement vector (MMV) problem with applications, for example, in distributed compressive sensing, direction-of-arrival estimation in radar, magnetic resonance imaging with multiple coils, diffuse optical tomography using multiple illumination patterns (see [13]–[15] and references therein).

The determination of sparse solutions for the MMV problem has been pursued actively in recent years. Relevant examples are greedy methods based on the simultaneous orthogonal matching pursuit [16]–[18], convex relaxation methods using mixed norms [12], [18]–[20], Bayesian methods enforcing a common sparsity profile via suitable prior [21], randomized methods [22], and model-based compressive sensing using block-sparsity [23], [24].

The designation "MMV problem" was coined with the advent of sparse regression in the nineties. However, the same problem, termed as *direction-of-arrival* (DOA) or the *bearing estimation problem* has been addressed since the seventies by the array signal processing community. The *multiple signal classification* (MUSIC) algorithm introduced independently in [25] and [26] is the most successful method to solve DOA problems. MUSIC first estimates an orthonormal basis for the signal subspace based on the empirical covariance matrix and then identifies the DOAs exploiting the fact that the vectors impinged on the array by the sources are orthogonal to the noise subspace. If the sources are uncorrelated (fractional abundances in our case) and the noise is Gaussian, independent (among sources and snapshots) and identically distributed (iid), the MUSIC estimator is a large sample realization (large number of spectral vectors in our case) of the maximum likelihood estimator [27]. In addition, in the absence of noise and if the rank of the observations is equal to the number of active elements in the support of vectors, the MUSIC yields perfect reconstruction [14].

When the rank of the observations is less than the number of active elements in the support of vectors, termed the "coherent source" problem within the sensor array signal processing context [28], the MUSIC algorithm fails. However, in this case the sparse regression algorithms are able to provide useful results even with just one observation. Several sufficient conditions for perfect reconstruction have been derived based on the the restricted isometric constants of the dictionary (see [14] and references therein).

In conclusion, we have two families of methods to solve the MMV problems. On the one hand, we have the sparse regression family, which is able to recover, at least in part, the support of the observed vectors, provided that the dictionary has suitable restricted isometric constants and regardless of the number of observations. On the other hand, we have the MUSIC based approaches, which yield very good results, provided that the rank of the observations is no less than the number of elements of the support of the vectors. Very recently, the complementarity between MUSIC and sparse regression approaches to solve MMV problems has been exploited [13], [14] by first applying sparse regression methods that identify a subset of the support and then apply MUSIC based methods. In this paper, we also exploit MUSIC and sparse regression approaches to unmix hyperspectral data, but in a reversed

order. Below, we detail our contribution.

B. Paper Contribution

In this paper we push forward the research boundary on hyperspectral sparse unmixing. We exploit a simple, yet fundamental, characteristic of hyperspectral data sets: the number of endmembers present in a given scene is often much less than the number of library signatures. Based on this characteristic, we introduce a two-step algorithm aimed at mitigating the aforementioned limitations of hyperspectral sparse unmixing. The first step starts by identifying the signal subspace and then runs a binary test over the library signatures to identify the endmembers. The signal subspace is estimated with the *Hyperspectral subspace identification by minimum error* (HySime) algorithm [29] and the binary test is similar to the MUSIC [25], [26] array signal processing algorithm. If the linear mixing model was an exact fit for observed spectral vectors and there was no noise, then the MUSIC step would, under mild assumptions, exactly identify the endmembers. However, we do have modeling errors and noise. Because of these degrading factors, the binary test in the MUSIC step is designed with a relative high false alarm probability yielding a set of signatures that, with high probability, contains the endmembers but is, nevertheless, much smaller than the complete library.

The second step is the collaborative sparse regression (CSR) algorithm introduced in [12] which, in addition to promoting joint sparsity over the abundance fraction vectors (*i.e.* collaborative sparseness), operates now on a pruned library. Because the dimensionality of the pruned library is, usually, much smaller than the dimensionality of the original library available, the conditioning of resulting sparse regression is naturally improved, and this has a strong positive impact on the quality of the obtained unmixing results as will be shown in this work.

The remainder of the paper is structured as follows. Section II introduces our MUSIC based approach to select a subset of the library signatures. Section III emphasizes recent developments in sparse unmixing. Section IV describes the proposed methodology. Section V analyzes the performance of the proposed approach with simulated data. Section VI discusses the performance with real hyperspectral data. Section VII concludes the paper with some remarks and hints at plausible future research lines.

II. The Multiple Measurement Problem

Let $\mathbf{y} \in \mathbb{R}^L$ denote an L-dimensional observed spectral vector from a given pixel of a hyperspectral image with L spectral bands and $\mathbf{A} := [\mathbf{a}_1, \ldots, \mathbf{a}_m] \in \mathbb{R}^{L \times m}$ denote a spectral library with m spectral signatures available *a priori*. Under the linear mixing model, the observed vector $\mathbf{y}$ can be expressed as a linear combination of spectral signatures taken from the library $\mathbf{A}$ as (see [5] for more details)

$$\mathbf{y} = \mathbf{A}\mathbf{x} + \mathbf{n}, \tag{1}$$

where the vector $\mathbf{x} \in \mathbb{R}^m$ holds the fractional abundances and the vector $\mathbf{n} \in \mathbb{R}^L$ holds the errors affecting the measurements at each spectral band. Because the abundance fractions are nonnegative and sum to one, the constraints $\mathbf{x} \geq \mathbf{0}$, to be understood in the component-wise sense, and $\mathbf{1}_m^T \mathbf{x} = 1$ ($\mathbf{1}_m$ stands for a column vector with m ones)

called abundance non-negativity constraint (ANC) and abundance sum-to-one constraint (ASC), respectively, are often imposed into the model (1).

Assuming that the data set contains $n \gg L$ pixels organized in the matrix $\mathbf{Y} := [\mathbf{y}_1, \ldots, \mathbf{y}_n]$, we can write

$$\mathbf{Y} = \mathbf{A}\mathbf{X} + \mathbf{N}, \tag{2}$$

where $\mathbf{X} := [\mathbf{x}_1, \ldots, \mathbf{x}_n]$ is the abundance fraction matrix and $\mathbf{N} := [\mathbf{n}_1, \ldots, \mathbf{n}_n]$ is the noise matrix. Let us assume momentarily that $\mathbf{N} = \mathbf{0}$ and disregard the ANC and the ASC. In these conditions, finding the sparsest common support for $\mathbf{x}_i$, with $i = 1, \ldots, n$, is precisely an MMV problem, which, formally, corresponds to finding the solution of the optimization

$$\begin{aligned} &\min_{\mathbf{X}} \|\mathbf{X}\|_0 \\ &\text{subject to: } \mathbf{Y} = \mathbf{A}\mathbf{X}, \end{aligned} \tag{3}$$

where $\|\mathbf{X}\|_0 := |S|$, $S := \text{supp}(\mathbf{X}) := \{1 \leq i \leq m \,:\, \mathbf{x}^i \neq \mathbf{0}\}$, and $\mathbf{x}^i$ is the ith row of $\mathbf{X}$.

The MMV problem (3) has a unique solution if and only if [30]

$$\|\mathbf{X}\|_0 < \frac{\text{spark}(\mathbf{A}) + \text{rank}(\mathbf{Y}) - 1}{2}, \tag{4}$$

where $\text{spark}(\mathbf{A})$ denotes the smallest number of linearly dependent columns of $\mathbf{A}$. The term $(\text{rank}(\mathbf{Y}) - 1)/2$ represents the MMV gain; that is, by increasing $\text{rank}(\mathbf{Y})$, which, under suitable conditions, is achieved by increasing the number of measurements, we are able to uniquely solve less sparse problems. Because $\text{rank}(\mathbf{Y}) \leq \|\mathbf{X}\|_0$, we have $\|\mathbf{X}\|_0 < \text{spark}(\mathbf{A}) - 1$.

When $\text{rank}(\mathbf{Y}) < \|\mathbf{X}\|_0$, the MMV problem is combinatorial and therefore very hard to solve exactly. As already referred to in Section I-A, the determination of sparse solutions for the MMV problem has been actively investigated in recent years (*e.g.* greedy, convex relaxation, Bayesian, randomized, block-sparsity methods). A much simpler scenario happens, however, when $\text{rank}(\mathbf{Y}) = \|\mathbf{X}\|_0 := k < L$. In this case, we can uniquely recover the support set $\text{supp}(\mathbf{X})$ as follows. Let us now write $\mathbf{Y} = \mathbf{A}_S\mathbf{X}^S$, where $\mathbf{A}_S \in \mathbb{R}^{L\times k}$ and $\mathbf{X}^S$ are the matrices holding, respectively, the columns of $\mathbf{A}$ and the rows of $\mathbf{X}$, whose indices are in S. Assuming that $\text{spark}(\mathbf{A}) > k + 1$ and that the rows of $\mathbf{X}^S$ are in general position, then $\mathbf{A}_S$ has full column rank and $\mathbf{X}^S$ has full row rank implying that $\text{range}(\mathbf{Y}) = \text{range}(\mathbf{A}_S)$. Therefore, an orthogonal basis for $\text{range}(\mathbf{A}_S)$ can be obtained from the singular value decomposition of $\mathbf{Y}$ or of $\mathbf{Y}\mathbf{Y}^T$. In the latter we have

$$\mathbf{Y}\mathbf{Y}^T = \mathbf{U}\,\text{diag}(\lambda_1, \ldots, \lambda_k)\,\mathbf{U}^T, \tag{5}$$

where $\mathbf{U} \in \mathbb{R}^{L\times k}$, $\mathbf{U}^T\mathbf{U} = \mathbf{I}_k$, $\lambda_1 \geq \lambda_2, \ldots, \lambda_k > 0$, and $\text{range}(\mathbf{U}) = \text{range}(\mathbf{A}_S)$. Now noting that $\mathbf{a}_j \in \text{range}(\mathbf{A}_S)$ if and only if (iff) $j \in S$ (otherwise we would have $\text{spark}(\mathbf{A}) \leq k + 1$), we conclude that

$$j \in S \quad \text{iff} \quad \mathbf{P}^{\perp}_{\mathbf{A}_S}\mathbf{a}_j = \mathbf{0}, \tag{6}$$

where $\mathbf{P}^{\perp}_{\mathbf{A}_S} := \mathbf{I} - \mathbf{U}\mathbf{U}^T$ is the projector on $\text{range}(\mathbf{A}_S)^{\perp}$. The equivalence (6) is the core of the MUSIC algorithm, which in its original version considers vectors $\mathbf{a}$ parameterized by continuous parameters representing DOAs, whereas in our hyperspectral application $\mathbf{a}$ is indexed by a finite index set.

In conclusion, we have proved the following result, which is a minor modification of Theorem 3.4 of [14]:

Theorem 1. Given the hyperspectral data set $\mathbf{Y} = \mathbf{AX} \in \mathbb{R}^{L\times n}$, with $\mathbf{X} \in \mathbb{R}^{m\times n}$, assume that rank$(\mathbf{Y}) = \|\mathbf{X}\|_0 := k < L$, spark$(\mathbf{A}) > k+1$, and the rows of $\mathbf{X}^S$ are in general position. Then, for $j \in \{1,\dots,n\}$, we have that $j \in$ supp$(\mathbf{X})$ iff $\mathbf{P}^{\perp}_{\mathbf{A}_S}\mathbf{a}_j = \mathbf{0}$. ■

A. Support Identification in the Presence of Noise

In real applications, we do have noise, *i.e.* $\mathbf{N} \neq \mathbf{0}$ in (2), which hinders the estimation of range$(\mathbf{A}_S)$. To shed light on the effect of noise, let us assume that the spectral vectors $\mathbf{y}_i$, for $i = 1,\dots,n$, are independent samples of a random $\mathbf{y}$ vector with correlation matrix $\mathbf{R}_y := \mathbb{E}[\mathbf{y}\mathbf{y}^T]$ and sample correlation matrix $\widehat{\mathbf{R}}_y := \mathbf{Y}\mathbf{Y}^T/n$. In these conditions, it can be easily concluded that $\mathbb{E}[\widehat{\mathbf{R}}_y - \mathbf{R}_y] = \mathbf{0}$ and that $\mathbb{E}[\|\widehat{\mathbf{R}}_y - \mathbf{R}_y\|^2] = \alpha/n$ for some $\alpha > 0$. Therefore, for n large enough, the sample correlation matrix $\widehat{\mathbf{R}}_y$ can be taken as a good approximation for the correlation matrix $\mathbf{R}_y$. Assuming that the noise and the fractional abundances are independent with correlation matrices $\mathbf{R}_n$ and $\mathbf{R}_x$, respectively, then it follows that

$$\mathbf{R}_y = \boldsymbol{A}_S\mathbf{R}_x(S)\boldsymbol{A}_S^T + \mathbf{R}_n, \tag{7}$$

where $\mathbf{R}_x(S)$ is the submatrix of $\mathbf{R}_x$ containing the rows and columns with indexes in S.

1) White Noise: If $\mathbf{R}_n = \sigma_n^2\mathbf{I}$, *i.e.,* the noise is iid, then the eigendecomposition of $\mathbf{R}_y$ is

$$\mathbf{R}_y = [\mathbf{U},\mathbf{V}]\,\mathrm{diag}(\lambda_1+\sigma_n^2,\dots,\lambda_k+\sigma_n^2,\sigma_n^2,\dots,\sigma_n^2)\,[\mathbf{U},\mathbf{V}]^T, \tag{8}$$

where λ_i, for $i = 1,\dots,k$ is the ith eigenvalue of $\boldsymbol{A}_S\mathbf{R}_x(S)\boldsymbol{A}_S^T$, $\mathbf{U} := [\mathbf{u}_1,\dots,\mathbf{u}_k]$ holds the first k eigenvectors of $\mathbf{R}_y$ and $\mathbf{V}$ holds the remaining eigenvalues. If $\mathbf{A}_S$ and $\mathbf{R}_x(S)$ are full rank, then $\lambda_i > 0$ for $i = 1,\dots,k$ and then range$(\mathbf{U})$ = range$(\mathbf{A}_S)$. In conclusion, if the noise is iid, then the signal subspace can be easily estimated from the sample correlation matrix $\widehat{\mathbf{R}}_y$, provided that n is large enough.

2) Colored or Correlated Noise: If $\mathbf{R}_n \neq \sigma_n^2\mathbf{I}$, the estimation of range$(\mathbf{A}_S)$ is hard because there is no more a simple relation between the eigenvectors of $\mathbf{R}_y$ and those of $\boldsymbol{A}_S\mathbf{R}_x(S)\boldsymbol{A}_S^T$ [31], [32]. Recently much attention has been devoted to the estimation of the noise covariance or correlation matrices in the context of DOA problems using for example autoregressive or autoregressive moving average models and parametric models [32]. A complementary approach focuses on properties of the signal assuming for example that it is non-Gaussian, or that its temporal correlation interval is significantly larger than that of noise , or assuming that the signals are linear combinations of a certain set of known basis functions [32].

In this paper, we adopt the HySime method [29] to estimate the signal subspace range$(\mathbf{A}_S)$. HySyme was conceived to exploit the characteristics of hyperspectral data sets. The method starts by estimating the noise correlation and the signal correlation matrices. The noise correlation matrix is estimated via multiple spectral band regression [33], which exploits the high correlation between neighboring spectral bands. HySime then selects the subset of eigenvectors that best represents the signal subspace in the minimum mean square error sense. The application of this criterion leads to the minimization of a two-term objective function. One term corresponds to

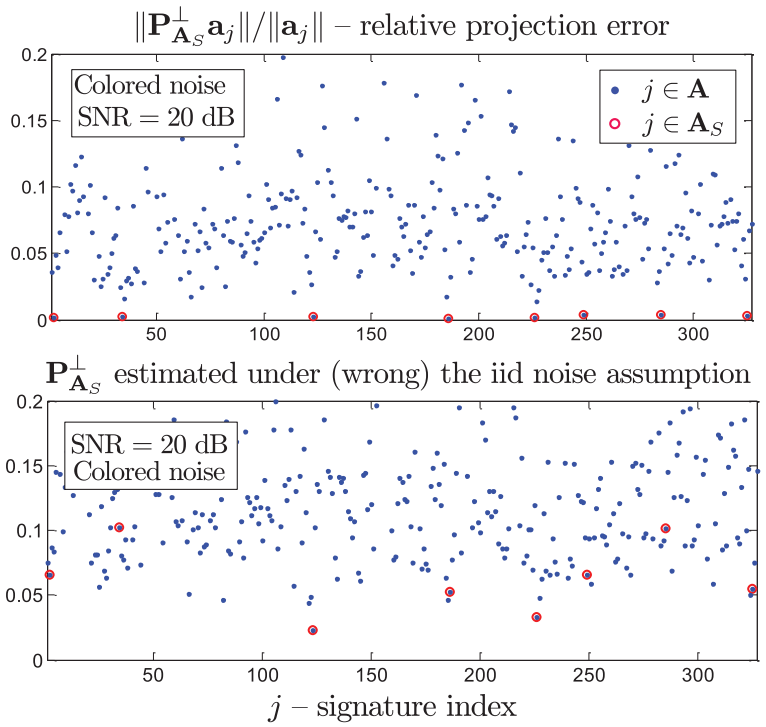

Fig. 1. Norm of projection of the spectral signatures onto the range$(\mathbf{A}_S)^{\perp}$ normalized by the norm of $\mathbf{a}_j$. The values corresponding to $j \in S$ (*i.e.*, the active spactral signatures) are circled. Top: range$(\mathbf{A}_S)^{\perp}$ based on the results yielded by the HySime algorithm, thus having into account that the noise is colored. Bottom: range$(\mathbf{A}_S)^{\perp}$ computed from the sample correlation matrix under the assumption that the noise is iid.

the power of the signal projection error and is a decreasing function of the subspace dimension; the other term corresponds to the power of the noise projection and is an increasing function of subspace dimension.

Figure 1 provides a numerical illustration of the proposed MUSIC based method and of the impact of (wrongly) assuming that the noise is iid, when in fact it is colored. We have generated a hyperspectral data set according to model (2) with $n = 100000$ hyperspectral vectors and library $\mathbf{A}$ formed by a subset of $m = 327$ spectral signatures of size $L = 224$ taken from the U.S. Geological Survey (USGS) splib06[3] library. The subset was chosen such that the angles between any two signatures are no smaller than 3 degrees. The fractional abundances are uniformly distributed over the simplex defined by the active spectral signatures in number of $k = 8$ taken randomly from $\mathbf{A}$. The noise $\mathbf{n}$ is Gaussian zero-mean independent from band to band and from vector to vector with a Gaussian shaped variance along the bands; the Gaussian shape is centered at the middle band and has a spread[4] of 20 bands. The signal-to-noise ratio (SNR $:= \mathbb{E}\,\|\mathbf{Ax}\|_2^2 \,/\mathbb{E}\,\|\mathbf{n}\|_2^2$) is set to 20 dB.

For each spectral signature $\mathbf{a}_j$, with $i = 1, \ldots, m$, we compute the norm of projection onto the range$(\mathbf{A}_S)^{\perp}$

[3]Available online: http://speclab.cr.usgs.gov/spectral.lib06

[4]Length of the interval between half variance bands.

normalized by the norm of $\mathbf{a}_j$:

$$\varepsilon_j := \frac{\|\mathbf{P}^{\perp}_{\mathbf{A}_S}\mathbf{a}_j\|_2}{\|\mathbf{a}_j\|_2}. \tag{9}$$

On the top of Fig. 1 the projection matrix $\mathbf{P}^{\perp}_{\mathbf{A}_S}$ was computed from the range$(\mathbf{A}_S)$ provided by the HySime algorithm. The eight smaller values of ε_i occur, as desirable, for $j \in S$. In contrast with this very good performance, some values of ε_i for $j \in S$ on the bottom of Fig. 1 are larger than many other errors for $j \notin S$. The reason for this poorer performance is the assumption that the noise is iid and, thus, computing the range$(\mathbf{A}_S)$ based on the sample correlation matrix as described in subsection II-A1.

III. Sparse Unmixing of Non-Negative Fractional Abundances Sharing the same Support

In the previous section, we showed that the active signatures $\mathbf{A}_S$ are effectively detected by the MUSIC algorithm adapted to the hyperspectral scenario. From $\mathbf{A}_S$, we can estimate the corresponding fractional abundances by solving, *e.g.*, the nonnegative constrained least squares (NCLS) optimization problem

$$\min_{\mathbf{Z}} \|\mathbf{Y} - \mathbf{A}_S\mathbf{Z}\|_F \tag{10}$$

$$\text{subject to: } \mathbf{Z} \geq \mathbf{0},$$

where $\|\mathbf{B}\|_F := \sqrt{\text{trace}\{\mathbf{B}\mathbf{B}^T\}}$. We have used the $\mathbf{Z} \in \mathbb{R}^{|S|\times n}$ instead of $\mathbf{X}^S$ to keep the notation light. Notice that we have not included the ASC $\mathbf{1}^T\mathbf{Z} = \mathbf{1}_n$ in (10) because it is hardly satisfied in real applications, namely owing to spectral variability. See [4] for more details.

In real hyperspectral imaging applications the detection of the support S is hindered by a few degradation mechanisms which include nonlinearities not captured by the linear model (1), calibration errors between the signatures available in the spectral library, and spectral variability within a given scene. These degradation mechanisms imply errors between the estimated range$(\mathbf{A}_S)$ inferred from the data $\mathbf{Y}$ and the subspace spanned by the corresponding elements in the library. These errors may lead to incorrect detection of the support S; that is, some of the k smaller indices ε_i given by (9) may correspond to inactive spectral signatures.

To avoid missing active signatures, we take a conservative approach by setting the probability of missing a signature to a low value. In doing so, we end up with a set R of cardinality $r := |R|$ larger than k but nevertheless much smaller than m, the number of signatures in library $\mathbf{A}$. In addition, we have with high probability $S \subset R$, *i.e.*, we do not miss any active signature. We will denote the reduced library with respect to R as $\mathbf{A}_R$.

The hyperspectral unmixing with respect to the $\mathbf{A}_R$, although a much simpler problem than the original one, is still not trivial because matrix $\mathbf{A}_R$ tends to be bad-conditioned. We attack this drawback by adding a regularization term to (10) which promotes sparsity among the rows of $\mathbf{Z}$. More specifically, we solve the optimization problem

$$\begin{aligned} \min_{\mathbf{Z}} \quad & \|\mathbf{Y} - \mathbf{A}_R\mathbf{Z}\|_F^2 + \lambda_C\|\mathbf{Z}\|_{2,1} \\ \text{subject to:} \quad & \mathbf{Z} \geq 0, \end{aligned} \tag{11}$$

where $\|\mathbf{Z}\|_{2,1} := \sum_{i=1}^{r} \|\mathbf{z}^i\|_2$ is the mixed $\ell_{2,1}$ norm, which promotes sparseness among the rows of $\mathbf{Z}$. Problem (11) is similar to the collaborative sparse coding problem described in [20], [34], [15], [35]. The main difference is the introduction of the constraint $\mathbf{Z} \geq 0$. Notice that the NCLS optimization (10) corresponds to (11) with $\lambda_C = 0$.

Let us assume that $r > L$, the noise is zero, and that we want to find the sparsest solution of $\mathbf{Y} = \mathbf{A}_R\mathbf{Z}$. In this case, it is shown in [15] that collaborative, or multichannel, sparse recovery yields a probability of recovery failure that decays exponentially in the number of channels. In other words, sparse methods have more chances to succeed when the number of acquisition channels increases. Herein, we summarize the results of Theorem [4.4] in [15], which assumes that the dictionary $\mathbf{A}_R$ is normalized and composed by i.i.d. Gaussian entries, the observations are generated by a set of atoms whose support is $S \subset \{1, 2, \ldots, m\}$ of cardinality k (*i.e.*, there are at most k rows in the solution matrix which are not identically zero) and $\left\|\mathbf{A}_S^{+}\mathbf{a}_l\right\|_2 \leq \alpha < 1$ holds for all $l \notin S$, where $\mathbf{A}_S^{+}$ is the pseudoinverse of the matrix $\mathbf{A}_S$ containing the atoms from $\mathbf{A}_R$ corresponding to the indices in S. The same theorem states that, under these assumptions, the solution $\mathbf{Z}$ of the linear system of equations $\mathbf{Y} = \mathbf{A}_R\mathbf{Z}$ is recovered by solving an $\ell_{2,1}$–norm optimization problem with probability at least $1 - m\exp\Big(-\frac{L}{2}(\alpha^{-2} - \log(\alpha^{-2}) - 1)\Big)$. The exponential decay of the error is obvious as $\alpha < 1$. Although the conditions from the aforementioned theorem are not met in common hyperspectral data, in which the dictionary atoms (that is, the pure spectral signatures) are highly correlated, leading to high values of $\left\|\mathbf{A}_S^{+}\mathbf{a}_l\right\|_2$, we have systematically observed the same type of behavior in our applications. Even when $r \leq L$, and thus the system matrix $\mathbf{Y} = \mathbf{A}_R\mathbf{Z}$ is determined or overdetermined, the inclusion of the $\ell_{2,1}$ regularizer in (11) has shown to be beneficial as is tends to set to zero the components of the rows of $\mathbf{Z}$ activated by the noise. In the next section, we give experimental evidence of the advantages of including the $\ell_{2,1}$ regularizer in (11). We compute the solution of (11) with the *Collaborative Sparse Unmixing algorithm via Variable Splitting and Augmented Lagrangian* (CLSUnSAL) algorithm [12]. CLSUnSAL is an elaboration of the Sparse Unmixing Algorithm via Variable Splitting and Augmented Lagrangian (SUnSAL) algorithm [36] designed to enforce the sparsity across pixel vectors. Both SUnSAL and CLSUnSAL exploit the alternating direction method of multipliers (ADMM) developed in [37] and originally introduced in [38].

IV. The MUSIC-CSR algorithm

In this section, we describe the proposed hyperspectral unmixing methodology via multiple signal classification and collaborative sparse regression, which we call MUSIC-CSR. Algorithm 1 shows MUSIC-CSR pseudocode. The inputs to the algorithm are a hyperspectral data set, $\mathbf{Y}$, a library holding the spectral signatures, $\mathbf{A}$, the number of signatures to be retained, *r*, and the regularization parameter, λ_C, for the CLSUnSAL algorithm. The output is a pruned library $\mathbf{A}_R$ with *r* signatures and the fractional signatures $\mathbf{X}^R$. Below, we summarize main steps of the MUSIC-CSR algorithm.

- *Signal Subspace (line 2)*: Infers the subspace in which the hyperspectral data $\mathbf{Y}$ lives. This is done using the HySime algorithm [29].
- *Projection errors (line 5)*: Computes the distance from each member of the library to the estimated subspace. The error indicator we use is the normalized Euclidean distance between one member of the library and the

Algorithm 1: MUSIC-CSR

Input: $\mathbf{A} \in \mathbb{C}^{L \times m}$ (library), $\mathbf{Y} \in \mathbb{R}^{L \times N}$ (hyperspectral image), r (number of signatures to be retained), λ_C (regularization parameter)

Output: $\mathbf{A}_R$ (detected signatures), $\mathbf{X}^R$ (fractional abundances with respect to $\mathbf{A}_R$)

1 **begin**

2 $\mathbf{E} := \text{HySime}(\mathbf{Y})$ (estimate an orthonormal basis for range$(\mathbf{A}_S)$ using the HySime algorithm [29])

3 $\mathbf{P}^{\perp}_{\mathbf{A}_S} := \mathbf{I} - \mathbf{E}\mathbf{E}^T$ (projector on range$(\mathbf{A}_S^{\perp})$)

4 **for** $i = 1$ **to** n **do**

5 $\varepsilon_j := \dfrac{\|\mathbf{P}^{\perp}_{\mathbf{A}_S}\mathbf{a}_j\|_2}{\|\mathbf{a}_j\|_2}$

6 $\pi := \text{permutation}\{1, \ldots, n \,:\, \varepsilon_{\pi(i)} \leq \varepsilon_{\pi(j)}, i \leq j\}$

7 $R := \{\pi(i),\, i = 1, \ldots, r\}$

8 Solve the collaborative sparse regression optimization

$$\mathbf{X}^R := \arg\min_{\mathbf{Z}} \quad \|\mathbf{Y} - \mathbf{A}_R\mathbf{Z}\|_F^2 + \lambda_C\|\mathbf{Z}\|_{2,1}$$
$$\text{subject to:} \quad \mathbf{Z} \geq 0,$$

using the CLSUnSAL algorithm [12].

estimated subspace in which the data lives.

- *Active set detection (lines 6 and 7)*: Sorts the normalized projection errors by increasing order and retain the indexes of first r in the set R.
- *Collaborative sparse regression optimization (line 8)*: Solve a collaborative sparse regression using the identified pruned library $\mathbf{A}_R$ using the CLSUnSAL algorithm [12].

In the following we illustrate the proposed MUSIC-CSR algorithm with a toy example. The dataset that we use in this example was generated using five randomly selected endmembers from a library containing 302 mineral spectra from the U.S. Geological Survey (USGS) library, denoted splib06[5], released in September 2007. The number of spectral bands is $L = 224$. We generated 5000 spectra by assuming that the fractional abundances follow a Dirichlet distribution. The datacube was contaminated with iid Gaussian noise. The variance was set to a value yielding SNR $= 20$ dB. This very high level of noise makes the problem very difficult.

In order to estimate the data subspace in this problem, we used the HySime algorithm which provided an estimated number of endmembers equal to five. The first five eigenvectors returned by HySime were used to define the subspace, and the library members were projected to the estimated subspace. For each member, the Euclidean distance to the subspace was then computed. Fig. 2 shows the obtained projection errors for all members. The errors

[5]Available online: http://speclab.cr.usgs.gov/spectral.lib06

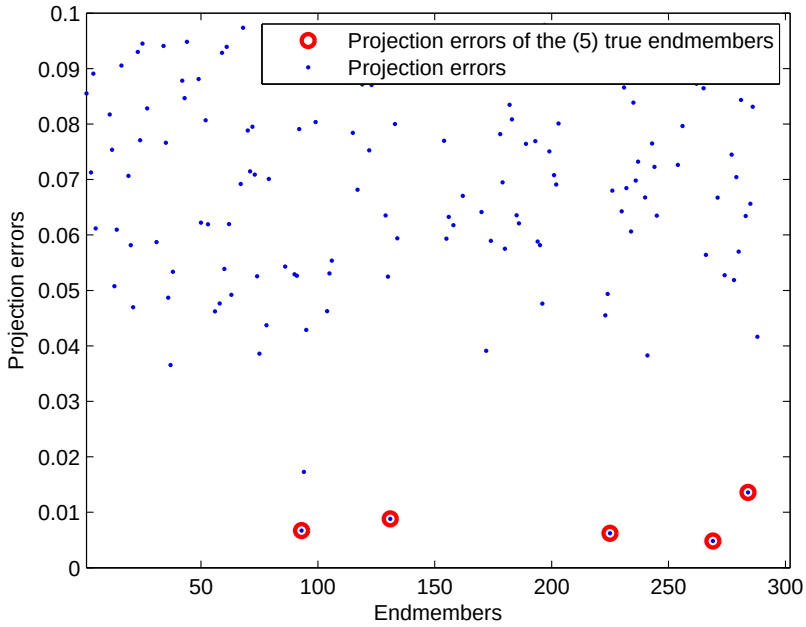

Fig. 2. Projection errors of the library members for the considered simulated toy example. The red circles show the projection errors of the true endmembers.

corresponding to true endmembers are highlighted with red circles. Note that these have the lowest projection errors among all the library members. The projection errors were then ordered in ascendent order so that the first five correspond to the true endmembers, as expected from Fig. 2. The reduced library $\mathbf{A}_R$ was then built by retaining the members corresponding to the lowest $r = 13$ projection errors, which correspond to a maximum allowed error of 0.045. The members are displayed in Fig. 3 (in this figure, the true endmembers are represented in black color). The mutual coherence of the obtained library (0.9983) was slightly lower than that of the original library (0.9986).

Finally the unmixing was performed using CLSUnSAL in two different situations: using $\mathbf{A}$ – *i.e.*, without pruning – (CSR) and using $\mathbf{A}_R$ – *i.e.*, after dictionary pruning – (MUSIC-CSR). Fig. 4(a) shows the true fractional abundances in the considered simulated toy example. Fig. 4(b) shows the cumulative abundance values (sum of the abundances for all pixels) corresponding to each endmember material. Fig. 4(c) shows the fractional abundances estimated by CSR with the cumulative abundance values displayed in Fig. 4(d). Finally, Fig. 4(e) shows the fractional abundances estimated by MUSIC-CSR with the cumulative abundance values displayed in Fig. 4(f). In all cases, the algorithm was tuned for optimal performance in the considered scenarios: the parameter λ_C was set to 0.1 for the unmixing cases using $\mathbf{A}$ and to 10^{-2} for the unmixing cases using $\mathbf{A}_R$.

From Fig. 4, we can conclude that the fractional abundances inferred by MUSIC-CSR are indeed closer to the true ones than those inferred by the CSR. The qualitative differences bewtween the two strategies can be appreciated both in the abundance plots and in the amplitude of the cumulative abundances. Most importantly, the MUSIC-

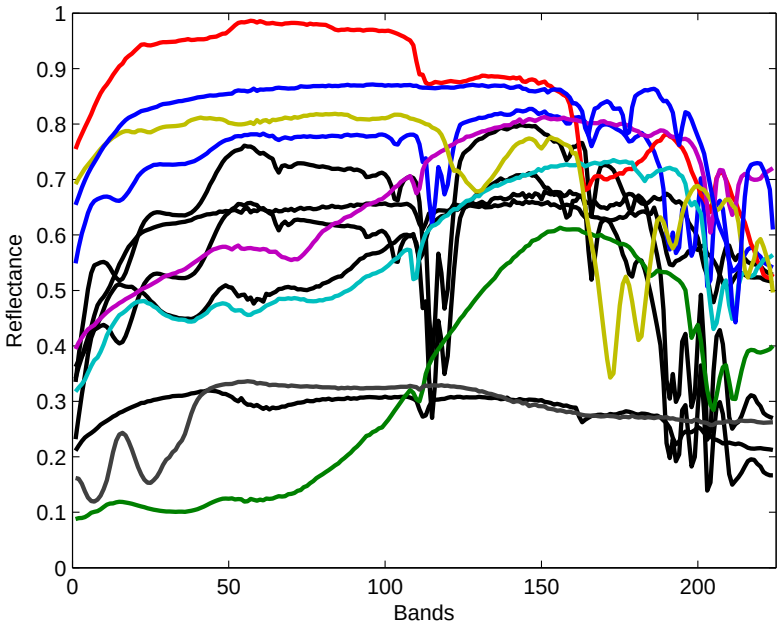

Fig. 3. Spectral signatures from the USGS spectral library which were retained after the pruning process.

CSR could properly identify the correct set of endmembers in order to explain the observed data. The positions of the true endmembers in the original library were: 93, 131, 225, 269 and 284. If we take into account only the highest 5 values of the cumulative abundances, Fig. 4 indicates that these correspond to the members: 94, 124, 166, 213 and 269 for the CSR and to members: 93, 131, 225, 269 and 284 for the MUSIC-CSR. As a result, the MUSIC-CSR is able to identify all the true endmembers that were used to generate the data, while the CSR could only identify correctly one of them. This is due to the fact that the original library contained groups of spectral signatures representing the same mineral.

V. Experimental Results Using Simulated Data

In this section, we test the effectiveness of the proposed dictionary pruning method in various simulated scenarios. The section is organized as follows. First, we describe the spectral libraries used in our simulated data experiments and the generated datasets. Then, we describe the considered performance discriminators. We use only datasets affected by noise, as the case in which the observations are not affected by noise is trivial. Next, the sparse unmixing methods presented in section III are applied to the simulated data sets using both the full library and pruned versions with different numbers of signatures (*i.e.*, in the latter case, step (8) of the MUSIC-CSR algorithm performs unmixing using also NCLS and SUnSAL algorithms, in order to exemplify the applicability of the proposed dictionary pruning methodology shown in steps (2)–(7) of the same algorithm in generic scenarios where per–pixel computation might be necessary). The obtained results are discussed from the viewpoint of estimation accuracy and

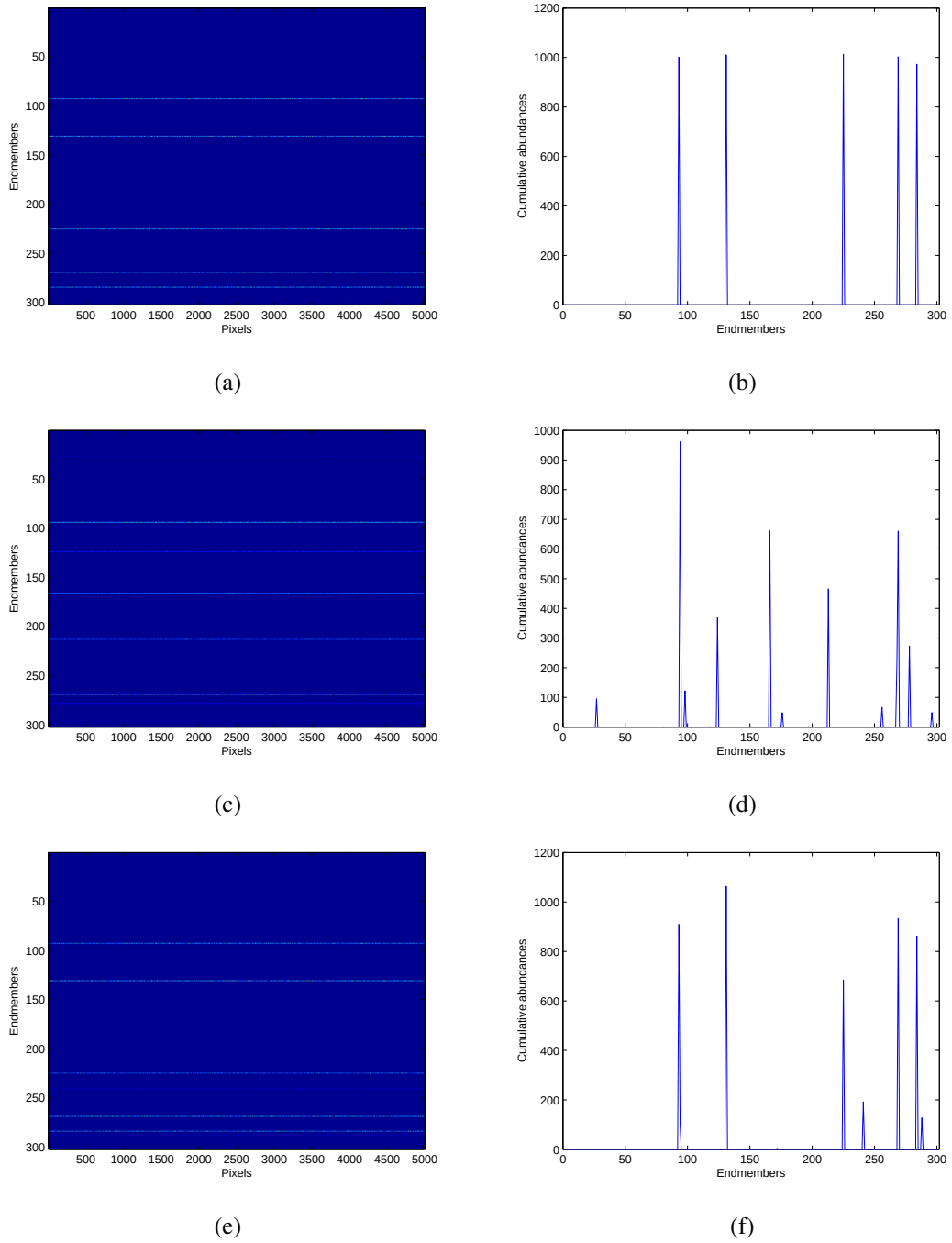

Fig. 4. (a) True fractional abundances in the considered simulated toy example. (b) Cumulative abundance values (sum of the abundances for all pixels) corresponding to each material. (c) Fractional abundances estimated by CSR. (d) Cumulative abundance values estimated using CSR. (e) Fractional abundances estimated by MUSIC-CSR. (f) Cumulative abundance values estimated using MUSIC-CSR.

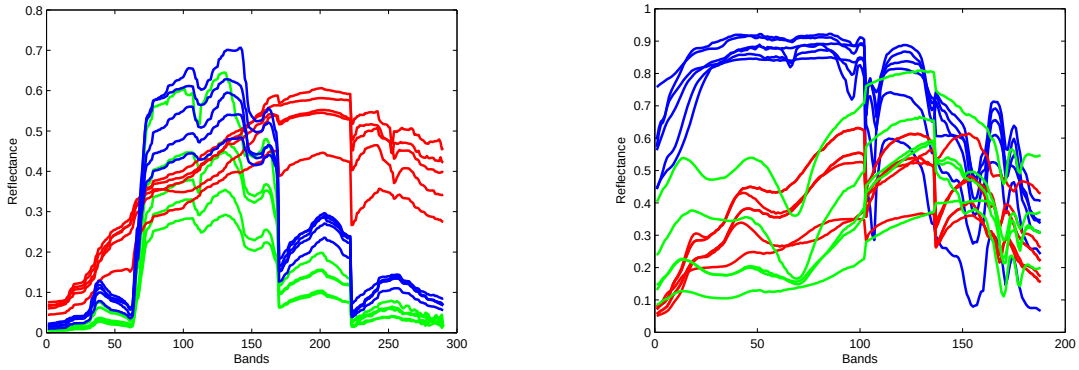

(a) $\mathbf{A}_1$ library with tree (green), weed (blue and soil (red) spectra.

(b) $\mathbf{A}_2$ library with actinolite (green), alunite (blue) and nontronite (red) spectra.

Fig. 5. (a) Five randomly selected spectral signatures from each class in spectral library $\mathbf{A}_1$. (b) Five randomly selected spectral signatures from each class in spectral library $\mathbf{A}_2$.

computational performance. The section concludes with a discussion on the most important observations resulting from the experiments conducted with simulated data.

A. Spectral Libraries

In our experiments with simulated data, we used two spectral libraries with very different characteristics. This allowed us to evaluate the proposed pruning methodology in different scenarios. In the following we provide a description of the two considered libraries.

- The first library, denoted hereinafter as $\mathbf{A}_1$, contains 50 soil, 200 citrus canopy, and 50 weed canopy reflectance spectra measured in a commercial Citrus orchard near Wellington, South Africa, using an Analytical Spectral Devices (ASD) field spectroradiometer with a 25° foreoptic, covering the 350–2500 nm spectral range. The library was compiled from field campaigns conducted at different periods during the growing season [39]. The major water absorption regions, sensitive to changing atmospheric water vapor content, were excluded from the analysis. Then, 290 spectral bands were randomly retained (out of 1798). This was done in order to deal with a very difficult problem, as in this case the mutual coherence of the library approaches one. The library is structured in three groups corresponding to the material classes: soil, citrus canopy, and weed. Fig. 5(a) plots five randomly selected spectral signatures contained in $\mathbf{A}_1$ for each class. Note that, while the soil signatures can be easily distinguished, confusions between the other two (vegetation) classes can easily occur.
- The second library, denoted hereinafter as $\mathbf{A}_2$ contains 240 randomly selected signatures from the USGS library, comprising different mineral types. The spectral signatures in this library are made up of reflectance values given in 224 spectral bands and distributed uniformly in the interval 400–2500 nm. The mutual coherence of $\mathbf{A}_2$ also approaches one. The library contains 55 groups of materials, each containing a variable number of signatures (between 1 and 17) describing different alterations of the same mineral. Fig. 5(b) plots five randomly selected spectral signatures contained in $\mathbf{A}_2$ for three different minerals: actinolite, alunite and notronite.

B. Simulated Data Cubes

The spectral libraries $\mathbf{A}_1$ and $\mathbf{A}_2$ were used to generate various simulated hyperspectral data sets. Specifically, three data cubes were generated using each library corresponding to different numbers of endmembers: $k = \{3, 6, 9\}$. The first three data cubes, denoted by DC1, DC2 and DC3, were generated using signatures from $\mathbf{A}_1$, while the other three data cubes, denoted by DC3, DC4 and DC6, were generated using signatures from $\mathbf{A}_2$. The endmembers were randomly selected as follows. In order to construct DC1, DC2 and DC3, we randomly selected one, two and three endmembers from each available class, respectively. The main reason for this selection was to avoid the case in which all the endmembers belong to the same class. On the other hand, at most one endmember was selected from each class in the construction of DC4, DC5 and DC6. This was done in order to avoid using more than one spectral signature for the same endmember. All the simulated data cubes comprised 5000 simulated spectra, where the fractional abundances of endmembers follow a Dirichlet distribution uniformly over the probability simplex [40]. The data cubes were then contaminated with white noise, using three levels of signal-to-noise ratio SNR: 30dB, 40dB and 50dB. For clarity, Table I shows the principal characteristics of the simulated data cubes.

TABLE I

MAIN CHARACTERISTICS OF THE SIX SIMULATED DATA CUBES CONSIDERED IN OUR STUDY

Simulated Data cube	**DC1**	**DC2**	**DC3**	**DC4**	**DC5**	**DC6**
Spectral library	$\mathbf{A}_1$	$\mathbf{A}_1$	$\mathbf{A}_1$	$\mathbf{A}_2$	$\mathbf{A}_2$	$\mathbf{A}_2$
Number of endmembers (k)	3	6	9	3	6	9
Number of pixels	5000	5000	5000	5000	5000	5000
SNR(dB)	30/40/50	30/40/50	30/40/50	30/40/50	30/40/50	30/40/50

C. Performance Discriminators

In our experiments we use several performance discriminators in order to substantiate the accuracy of the sparse unmixing process, with and without dictionary pruning. An important parameter for the pruned libraries is the number of the correctly retained endmembers and their projection errors, which will be given for all our tests. Regarding the quality of the reconstruction of spectral mixtures, the performance discriminator adopted in this work is the signal to reconstruction error [5]: SRE $\equiv \mathbb{E}[\|\mathbf{x}\|_2^2]/\mathbb{E}[\|\mathbf{x} - \widehat{\mathbf{x}}\|_2^2]$, measured in dB: SRE(dB) $\equiv 10\log_{10}(\text{SRE})$. We use this measure instead of the root mean square error (RMSE) [41] as it gives more information regarding the power of the error in relation with the power of the signal. The higher the SRE(dB), the better the unmixing performance. We also computed a so-called "probability of success," p_s, which is an estimate of the probability that the relative error power be smaller than a certain threshold. This metric is a widespread one in sparse regression literature, and is formally defined as follows: $p_s \equiv P(\|\widehat{\mathbf{x}} - \mathbf{x}\|^2/\|\mathbf{x}\|^2 \leq threshold)$. This performance measure gives an indication about the stability of the estimation that is not inferable directly from the SRE (which is an average).

In this work, as we are more interested in finding the correct fractional abundances of the endmember classes (not necessarily of a specific member of the library), we will consider also the case in which the abundance of one

endmember is represented by the sum of abundances of all the members of the class (group of materials) associated to the endmember. In other words, we highlight the performance indicators not only for the individual members of the library (i.e., *per member* assessment), but also for each group considered as an unique endmember (i.e., *per group* assessment). In the former case, the *threshold* value used to compute the p_s is set to 5dB. This is because we have shown in previous work that solutions attaining this value can be considered of high quality [5]. On the other hand we also emphasize that, when computing the p_s metric *per group*, most of the unmixing results lead to higher SRE(dB). This means that the p_s is equal or very close to one. In this situation, we set a higher quality threshold of 15dB. By doing this, we can better discriminate between the accuracy achieved by different sparse unmixing methods. The computation times will be also reported for all our experiments.

D. Performance Evaluation

The proposed dictionary pruning methodology was applied to the simulated data cubes by retaining different numbers of signatures $r = \{20, 40, 60\}$. The algorithms discussed in section III were used to solve the unmixing problem with the full and with the pruned libraries. All algorithms (except NCLS which is parameter-free) were tuned empirically for optimal performance by carefully adjusting the parameters in each test and reporting only the best obtained results. Four different experiments have been conducted, intended to analyze the quality of the selected endmembers after pruning, the quality of the estimated fractional abundances per member and per group, and the computational performance of the different techniques tested.

TABLE II

NUMBER OF CORRECTLY EXTRACTED MEMBERS FROM THE ORIGINAL LIBRARIES AFTER THE PRUNING PROCESS USING SIMULATED DATA CUBES CONSTRUCTED USING DIFFERENT SIGNAL-TO-NOISE RATIO (SNR) VALUES

Data Cube (true number of endmembers)	**Size of the library after pruning**	**SNR=30dB**	**SNR=40dB**	**SNR=50dB**
DC1 (3)	20	3	3	3
	40	3	3	3
	60	3	3	3
DC2 (6)	20	6	6	6
	40	6	6	6
	50	6	6	6
DC3 (9)	20	7	9	9
	40	9	9	9
	60	9	9	9
DC4 (3)	20	3	3	3
	40	3	3	3
	60	3	3	3
DC5 (6)	20	6	6	6
	40	6	6	6
	50	6	6	6
DC6 (9)	20	8	9	9
	40	9	9	9
	50	9	9	9

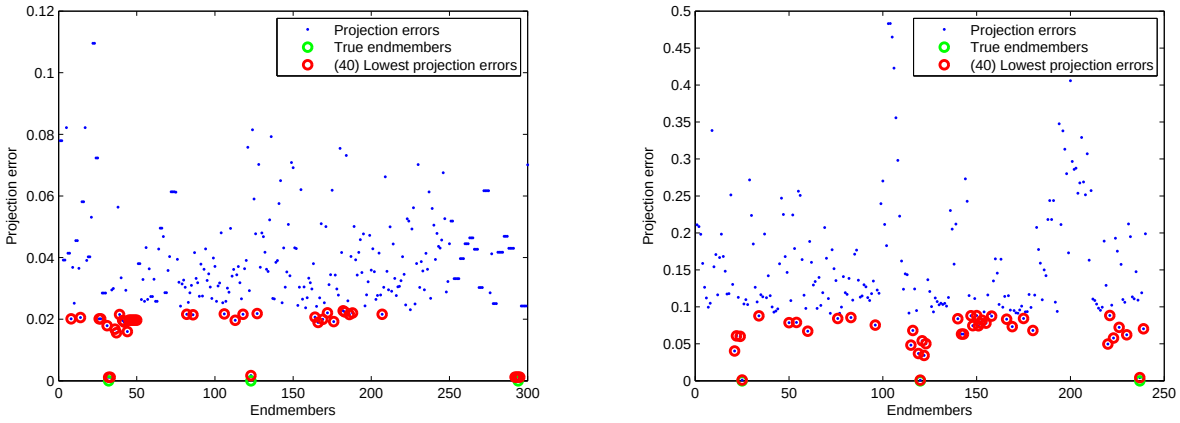

(a) DC1 (b) DC4

Fig. 6. Projection errors for the members of $\mathbf{A}_1$ and $\mathbf{A}_2$, when the simulated datacubes DC1 and DC4 are contaminated with noise having SNR=30dB and 40 members from each library are retained in the pruning process.

1) Experiment 1: Quality of Selected Endmembers After Pruning: Table II shows the number of correctly selected members from the original spectral libraries after the pruning process. From Table II, it can be seen that the proposed pruning method is able to identify the correct endmembers in most cases. Only some difficulties were encountered in situations in which the number of endmembers is high ($k = 9$) and the SNR is very low (30dB). On the other hand, the method is able to retain correctly all the endmembers when the SNR is higher than 40dB, which is a reasonable SNR level in most hyperspectral applications. On the other hand, Fig. 6 illustrates the projection errors measured for the members of $\mathbf{A}_1$ and $\mathbf{A}_2$ after analyzing the data cubes DC1 and DC4, respectively. In the figure, the projection errors measured for the retained endmembers are highlighted with red circles, while the green circles indicate the position of the actual endmembers. From Fig. 6, it can be concluded that the true endmembers always exhibit very low projection errors. Although $\mathbf{A}_1$ is characterized by a high variability of the three classes of endmembers, only a few members are really close to the inferred subspace. Despite $\mathbf{A}_2$ is more heterogeneous (i.e., it contains a larger number of classes as compared to $\mathbf{A}_1$), a clear gap can be observed in the projection errors measured for the true endmembers and those measured for the other members in the library. This confirms the results reported on Table II.

2) Experiment 2: Accuracy of Estimated Abundances Per Member: Table III shows the SRE(dB) and the p_s achieved by the considered unmixing techniques *per member* for the simulated data cubes generated using the library $\mathbf{A}_1$. Similarly, Table IV shows the same performance indicators for the simulated data cubes generated using $\mathbf{A}_2$. From Tables III and IV, it can be seen that the SRE(dB) and p_s values computed *per member* are generally higher for $\mathbf{A}_2$. This is because $\mathbf{A}_2$ is more heterogeneous in nature than $\mathbf{A}_1$. As expected, the methods which enforce sparsity explicitly (SUnSAL and CLSUnSAL) perform better than NCLS. In general, the performances of all the algorithms improve systematically after dictionary pruning. Not surprisingly, the performances of the algorithms

TABLE III

SRE(DB) AND p_s PER MEMBER BY THE CONSIDERED UNMIXING TECHNIQUES FOR SIMULATED DATA CUBES: DC1, DC2 AND DC3

SRE(dB)										
Method	Library size	DC1 ($k = 3$)			DC2 ($k = 6$)			DC3 ($k = 9$)		
		SNR=30dB	SNR=40dB	SNR=50dB	SNR=30dB	SNR=40dB	SNR=50dB	SNR=30dB	SNR=40dB	SNR=50dB
NCLS	300 (full)	1.25	3.27	3.77	0.10	2.75	4.07	-0.78	0.93	2.58
	60	2.23	3.57	3.82	1.25	3.47	4.26	0.39	2.17	3.45
	40	2.53	3.63	3.82	1.40	3.52	4.27	1.22	2.74	3.56
	20	2.82	3.69	3.83	2.20	3.91	4.34	1.35	3.51	3.75
SUnSAL	300 (Full)	1.44	3.28	3.78	1.19	3.22	4.10	-0.25	0.97	2.76
	60	2.26	3.57	3.82	2.21	3.91	4.26	0.76	2.17	3.45
	40	2.56	3.63	3.82	2.71	4.06	4.34	1.36	2.74	3.56
	20	2.94	3.69	3.83	3.21	4.21	4.36	1.36	3.51	3.75
CLSUnSAL	300 (Full)	2.78	3.68	3.83	2.57	4.05	4.36	0.61	1.86	3.35
	60	3.08	3.73	3.84	3.46	4.21	4.38	2.14	3.20	3.67
	40	3.19	3.75	3.84	3.80	4.26	4.39	2.59	3.36	3.69
	20	3.43	3.78	3.84	3.92	4.32	4.40	1.49	3.54	3.75
p_s										
Method	Library size	DC1 ($k = 3$)			DC2 ($k = 6$)			DC3 ($k = 9$)		
		SNR=30dB	SNR=40dB	SNR=50dB	SNR=30dB	SNR=40dB	SNR=50dB	SNR=30dB	SNR=40dB	SNR=50dB
NCLS	300 (Full)	0.09	0.25	0.31	0.04	0.19	0.39	0	0.01	0.08
	60	0.15	0.29	0.32	0.10	0.30	0.41	0.02	0.08	0.22
	40	0.18	0.29	0.32	0.12	0.30	0.41	0.05	0.12	0.24
	20	0.22	0.30	0.32	0.22	0.36	0.42	0.02	0.22	0.27
SUnSAL	300 (Full)	0.10	0.25	0.31	0.08	0.25	0.39	0	0.02	0.12
	60	0.15	0.29	0.32	0.14	0.36	0.41	0.03	0.08	0.22
	40	0.19	0.29	0.32	0.19	0.38	0.42	0.05	0.12	0.24
	20	0.23	0.30	0.32	0.29	0.40	0.42	0.05	0.22	0.27
CLSUnSAL	300 (Full)	0.21	0.30	0.32	0.13	0.38	0.42	0	0.02	0.20
	60	0.23	0.31	0.32	0.27	0.41	0.43	0.04	0.17	0.25
	40	0.25	0.31	0.32	0.35	0.41	0.43	0.10	0.19	0.26
	20	0.28	0.31	0.32	0.37	0.42	0.43	0.03	0.23	0.27

improve when the retained number of signatures approaches the true number of endmembers for both $\mathbf{A}_1$ and $\mathbf{A}_2$. The only exception corresponds to the simulated data cube DC3 (using $\mathbf{A}_1$), in which only 20 members from the original library are retained. However, this behavior is not related to the pruning methodology itself but to the ability of the chosen subspace estimator (in our case, the HySime method) to infer the correct subspace in such environment affected by strong signature variability. Moreover, the spectral confusion between the endmembers is high in this particular case since DC3 was generated using three signatures from each available classes of materials (soil, tree, weed). The same decrease in terms of accuracy is observed for DC5 and DC6 when the observations are affected by high noise (SNR=30dB) and only 20 members of the original library were retained. Even so, it can be observed that the unmixing results for any pruning level improve in terms of accuracy when compared to the results obtained with the original library. It should be noted that SNR values of 30dB are not typically encountered in practice since modern hyperspectral instruments provide high SNR values [42]. Another important observation from Tables III and IV is that the considered unmixing algorithms perform better when the number of endmembers in the image is low (see results for DC1 and DC4). This was already observed in the original sparse unmixing formulation [5]. After analyzing the accuracy of the unmixing results computed *per member*, we conclude that dictionary pruning can significantly improve the obtained unmixing accuracies in most cases.

3) Experiment 3: Accuracy of Estimated Abundances Per Group: Table V shows the SRE(dB) and the p_s achieved by the considered unmixing techniques *per group* for the simulated data cubes generated using the library $\mathbf{A}_1$. Similarly, Table VI shows the same performance indicators for the simulated data cubes generated using $\mathbf{A}_2$.

TABLE IV

SRE(DB) AND p_s PER MEMBER BY THE CONSIDERED UNMIXING TECHNIQUES FOR SIMULATED DATA CUBES: DC4, DC5 AND DC6

SRE(dB)										
Method	Library size	DC4 ($k = 3$)			DC5 ($k = 6$)			DC6 ($k = 9$)		
		SNR=30dB	SNR=40dB	SNR=50dB	SNR=30dB	SNR=40dB	SNR=50dB	SNR=30dB	SNR=40dB	SNR=50dB
NCLS	240 (Full)	7.86	15.60	21.62	0.77	4.53	9.24	0.25	3.91	8.80
	60	9.70	18.59	28.25	3.45	8.43	15.46	4.52	10.45	18.48
	40	12.63	21.66	31.18	3.53	8.77	16.08	5.46	11.62	19.90
	20	14.01	23.09	32.60	5.07	11.20	19.05	4.79	13.23	21.54
SUnSAL	240 (Full)	7.96	16.06	25.66	1.82	5.75	11.16	1.39	4.25	10.20
	60	10.30	18.59	28.25	3.45	8.43	15.46	4.52	10.45	18.48
	40	12.63	21.66	31.18	3.54	8.77	16.08	5.46	11.62	19.90
	20	14.01	23.09	32.60	5.07	11.20	19.05	4.87	13.23	21.54
CLSUnSAL	240 (Full)	9.62	17.77	27.69	3.51	8.03	15.77	2.75	6.39	12.55
	60	13.33	22.26	31.81	5.80	11.54	18.43	6.37	12.50	20.44
	40	13.41	22.37	31.86	6.02	12.06	19.15	6.71	13.15	21.49
	20	14.34	23.43	32.90	8.89	13.92	20.98	5.76	14.86	23.53
p_s										
Method	Library size	DC4 ($k = 3$)			DC5 ($k = 6$)			DC6 ($k = 9$)		
		SNR=30dB	SNR=40dB	SNR=50dB	SNR=30dB	SNR=40dB	SNR=50dB	SNR=30dB	SNR=40dB	SNR=50dB
NCLS	240 (Full)	0.83	1.00	1.00	0.14	0.51	0.97	0.08	0.42	0.96
	60	0.92	1.00	1.00	0.38	0.88	1.00	0.51	0.97	1.00
	40	0.99	1.00	1.00	0.40	0.90	1.00	0.63	0.99	1.00
	20	1.00	1.00	1.00	0.59	0.96	1.00	0.58	0.99	1.00
SUnSAL	240 (Full)	0.84	1.00	1.00	0.20	0.64	0.99	0.11	0.45	0.99
	60	0.94	1.00	1.00	0.38	0.88	1.00	0.51	0.97	1.00
	40	0.99	1.00	1.00	0.40	0.90	1.00	0.63	0.99	1.00
	20	1.00	1.00	1.00	0.59	0.96	1.00	0.58	0.99	1.00
CLSUnSAL	240 (Full)	0.96	1.00	1.00	0.36	0.91	1.00	0.18	0.75	1.00
	60	1.00	1.00	1.00	0.65	1.00	1.00	0.75	1.00	1.00
	40	1.00	1.00	1.00	0.69	1.00	1.00	0.78	1.00	1.00
	20	1.00	1.00	1.00	0.91	1.00	1.00	0.68	1.00	1.00

We recall that, in this case, the threshold used to compute p_s was set to 15, which decreases the probability of this performance discriminator to approach one. Tables V and VI are consistent with our observations related to the performance discriminators computed *per member*. Specifically, we can observe improvements in unmixing performance in all cases, particularly when the noise levels are not very high. For the cases with a low number of endmembers in the original data, the probability of success approaches optimal performance (see DC1 and DC4). The low p_s observed in some cases is due to the high threshold set in computing this performance measure. At the same time, the values of SRE(dB) are generally higher than 5dB (this value corresponds to high quality in the estimation of the fractional abundances). On the other hand, the unmixing results obtained with pruned libraries are always more accurate than those obtained with the corresponding full library. This is particularly the case for the simulations using $\mathbf{A}_2$ as the baseline library.

4) Experiment 4: Computational Performance of the Considered Algorithms: Table VII reports the computation times measured for the considered algorithms. The times are expressed in milliseconds and correspond to the average running times, per pixel, for fixed values of the regularization parameters ($\lambda = \lambda_C = 10^{-4}$). The maximum number of iterations was set to 1000 in all cases. The NCLS solution was calculated using the SUnSAL algorithm, by setting the regularization parameter to $\lambda = 0$. The algorithms were executed on a desktop PC with an Intel Core Duo CPU @2.5GHz and 4GB of RAM memory. The times reported for the unmixing algorithms with dictionary pruning already include the computation time of the pruning process. From Table VI, we can conclude that a significant decrease in computation time can be observed for all algorithms when dictionary pruning is performed. In some

TABLE V

SRE(dB) AND p_s PER GROUP BY THE CONSIDERED UNMIXING TECHNIQUES FOR SIMULATED DATA CUBES: DC1, DC2 AND DC3

SRE(dB)										
Method	Library size	DC1 ($k = 3$)			DC2 ($k = 6$)			DC3 ($k = 9$)		
		SNR=30dB	SNR=40dB	SNR=50dB	SNR=30dB	SNR=40dB	SNR=50dB	SNR=30dB	SNR=40dB	SNR=50dB
NCLS	300 (Full)	9.06	16.66	24.77	7.93	14.57	22.31	9.22	14.12	19.66
	60	18.27	27.31	37.21	12.92	19.51	28.10	13.08	19.37	28.46
	40	18.58	27.70	37.67	12.88	19.71	28.29	14.04	21.43	30.00
	20	17.89	27.03	36.94	13.93	21.78	30.92	9.83	23.34	32.53
SUnSAL	300 (Full)	11.44	16.84	26.17	12.26	20.66	21.13	8.66	11.22	17.29
	60	19.28	27.31	37.21	12.71	23.61	26.34	11.34	16.34	25.43
	40	19.91	27.70	37.67	13.13	22.28	28.51	11.82	18.40	26.97
	20	19.97	27.03	36.94	17.12	25.49	28.82	8.80	20.31	29.50
CLSUnSAL	300 (Full)	13.80	22.57	32.20	14.67	22.63	31.52	9.51	13.34	21.58
	60	19.80	29.46	38.80	17.14	25.65	34.20	12.37	18.26	26.89
	40	20.60	30.00	39.59	17.85	25.98	35.22	12.67	19.29	27.12
	20	21.24	30.66	40.35	17.92	26.45	35.39	10.83	20.50	29.51
p_s										
Method	Library size	DC1 ($k = 3$)			DC2 ($k = 6$)			DC3 ($k = 9$)		
		SNR=30dB	SNR=40dB	SNR=50dB	SNR=30dB	SNR=40dB	SNR=50dB	SNR=30dB	SNR=40dB	SNR=50dB
NCLS	300 (Full)	0.33	0.75	1.00	0.27	0.61	0.99	0.31	0.59	0.94
	60	0.86	1.00	1.00	0.60	0.90	1.00	0.55	0.91	1.00
	40	0.87	1.00	1.00	0.60	0.91	1.00	0.63	0.97	1.00
	20	0.86	1.00	1.00	0.70	0.95	1.00	0.37	0.99	1.00
SUnSAL	300 (Full)	0.49	0.76	1.00	0.57	0.99	0.99	0.30	0.60	0.95
	60	0.90	1.00	1.00	0.64	1.00	1.00	0.59	0.91	1.00
	40	0.92	1.00	1.00	0.65	1.00	1.00	0.65	0.97	1.00
	20	0.92	1.00	1.00	0.89	1.00	1.00	0.31	0.99	1.00
CLSUnSAL	300 (Full)	0.60	0.99	1.00	0.77	1.00	1.00	0.42	0.78	1.00
	60	0.92	1.00	1.00	0.89	1.00	1.00	0.69	0.98	1.00
	40	0.95	1.00	1.00	0.93	1.00	1.00	0.72	0.99	1.00
	20	0.96	1.00	1.00	0.93	1.00	1.00	0.44	0.99	1.00

cases, the decrease is weakly correlated with the number of members retained from the original library (see, for example, the computation times measured for the SUnSAL method applied to the data cubes generated using $\mathbf{A}_1$). This is because, when the library is pruned, not only the number of computations decreases dramatically but also the algorithms converge faster. As a result, in this case the algorithms do not reach the imposed limit of 1000 iterations. This is a very encouraging result, which further confirms the advantages that can be gained by applying the proposed methodology.

Summarizing, in this section we have conducted extensive tests to evaluate the potential of the proposed dictionary pruning methodology using simulated data sets. The libraries used in our tests exhibit distinct characteristics with regards to the type of materials represented in those libraries. While $\mathbf{A}_1$ contains three groups of signatures, corresponding to soil, citrus canopy and weed, $\mathbf{A}_2$ contains 55 groups of mineral signatures. Our results indicate that dictionary pruning significantly improves the unmixing results in all cases, both in terms of the accuracy of the solutions and the time to obtain them. The accuracy of the solutions always improved after the pruning process, regardless of whether they were computed *per member* or *per group*. We have also shown that dictionary pruning allows unmixing algorithms to converge faster to optimal solutions. Although our results with computer simulations are encouraging, further experiments with real hyperspectral data should be conducted.

VI. EXPERIMENTAL RESULTS USING REAL DATA

This section exemplifies the applicability of the proposed dictionary pruning methodology in real environments. In our previous work [43], we conducted a qualitative evaluation of the proposed pruning methodology using the

TABLE VI

SRE(dB) AND p_s PER GROUP BY THE CONSIDERED UNMIXING TECHNIQUES FOR SIMULATED DATA CUBES: DC4, DC5 AND DC6

SRE(dB)										
Method	Library size	DC4 ($k = 3$)			DC5 ($k = 6$)			DC6 ($k = 9$)		
		SNR=30dB	SNR=40dB	SNR=50dB	SNR=30dB	SNR=40dB	SNR=50dB	SNR=30dB	SNR=40dB	SNR=50dB
NCLS	240 (Full)	8.40	16.14	22.07	2.48	6.28	10.97	1.20	4.90	9.94
	60	10.18	19.01	28.69	7.14	13.61	21.38	6.13	12.78	21.18
	40	13.63	22.59	32.10	7.34	13.83	21.73	7.39	14.19	22.62
	20	15.15	24.12	33.62	10.07	20.26	28.58	6.45	15.85	24.38
SUnSAL	240 (Full)	8,39	16,60	26,23	4,61	8,60	13,64	2,91	5,96	11,35
	60	10,88	19,01	28,69	7,87	14,28	22,05	6,13	12,78	21,18
	40	13,63	22,59	32,10	8,08	14,50	22,40	7,39	14,19	22,62
	20	15,15	24,12	33,62	10,85	20,93	29,25	6,52	15,85	24,38
CLSUnSAL	240 (Full)	9,84	18,20	27,94	5,94	10,22	18,82	4,01	7,76	13,91
	60	14,03	23,16	32,47	9,39	16,66	24,51	7,77	14,37	22,73
	40	14,24	23,35	32,60	11,25	17,99	25,15	8,62	15,38	23,80
	20	15,23	24,39	34,10	15,07	21,99	30,10	7,43	16,99	25,83
p_s										
Method	Library size	DC4 ($k = 3$)			DC5 ($k = 6$)			DC6 ($k = 9$)		
		SNR=30dB	SNR=40dB	SNR=50dB	SNR=30dB	SNR=40dB	SNR=50dB	SNR=30dB	SNR=40dB	SNR=50dB
NCLS	240 (Full)	0.15	0.71	0.99	0.01	0.13	0.35	0	0.01	0.10
	60	0.34	0.89	1,00	0.09	0.54	0.99	0.02	0.35	0.99
	40	0.54	0.99	1.00	0.12	0.58	0.99	0.06	0.52	1.00
	20	0.66	1.00	1.00	0.36	0.96	1.00	0.09	0.71	1.00
SUnSAL	240 (Full)	0.14	0.74	1.00	0.02	0.22	0.53	0	0.02	0.21
	60	0.35	0.89	1.00	0.09	0.54	0.99	0.02	0.35	0.99
	40	0.54	0.99	1.00	0.12	0.58	0.99	0.06	0.52	1.00
	20	0.66	1.00	1.00	0.36	0.96	1.00	0.08	0.71	1.00
CLSUnSAL	240 (Full)	0.19	0.88	1.00	0.05	0.40	0.93	0	0.03	0.41
	60	0.57	0.99	1.00	0.09	0.77	1.00	0.02	0.49	1.00
	40	0.58	0.99	1.00	0.22	0.89	1.00	0.05	0.64	1.00
	20	0.66	1.00	1.00	0.62	0.99	1.00	0.12	0.80	1.00

well-known Cuprite data set collected by the Airborne Visible Infra-Red Imaging Spectrometer (AVIRIS), which is available online in reflectance units[6]. The aforementioned real data experiment is related to the tests conducted in section V with the $\mathbf{A}_2$ library, in which a dictionary composed entirely of mineral signatures was used. The results included in [43] demonstrated that the unmixing results (obtained with both NCLS and SUnSAL algorithms) were correlated with the ground-truth data available, and the minerals of interest exhibited good spatial distribution. In that scene, a quantitative evaluation was not possible, as the ground-truth information available is a classification map obtained by the USGS Tricorder algorithm, in which each pixel is assigned to a certain endmember class without providing information about the fractional abundance of each endmember.

In this work, we use a different real hyperspectral data set for which the true fractional abundances of endmembers are available. The data set comprises *in situ* measurements of reflectance spectra collected over mixed ground plots (i.e., covered by more than one material class) in a commercial Citrus orchard near Wellington, South Africa. Mixed pixel spectra were measured for different material class combinations: (i) tree-soil; (ii) tree-weed; (iii) tree-soil-weed. For each mixture combination, 25 mixed pixel spectra were measured. For each pixel, specific endmember spectra and ground cover fraction distributions were determined. The reflectance spectra were measured from nadir at a height of 4 m using an ASD field spectroradiometer with a 25 foreoptic, covering the 350–2500 nm spectral range. The major water absorption regions, sensitive to changing atmospheric water vapor content, were excluded from the analysis, thus obtaining a dataset with 1798 spectral bands. The plot-specific endmembers were acquired

[6]http://aviris.jpl.nasa.gov/html/aviris.freedata.html

TABLE VII

COMPUTATION TIMES (MILLISECONDS) FOR THE UNMIXING ALGORITHMS, WITH AND WITHOUT PRUNING, IN SIMULATED EXPERIMENTS

Spectral library: $\mathbf{A}_1$										
Method	Library size	DC1 ($k = 3$)			DC2 ($k = 6$)			DC3 ($k = 9$)		
		SNR=30dB	SNR=40dB	SNR=50dB	SNR=30dB	SNR=40dB	SNR=50dB	SNR=30dB	SNR=40dB	SNR=50dB
NCLS	240 (Full)	12.95	13.86	12.86	13.04	8.52	8.25	13.61	4.24	4.21
	60	1.26	1.21	0.49	0.86	0.39	0.47	0.49	0.40	0.53
	40	0.78	0.89	0.27	0.58	0.26	0.27	0.25	0.26	0.24
	20	0.52	0.42	0.18	0.26	0.12	0.17	0.12	0.13	0.15
SUnSAL	240 (Full)	15.39	15.64	14.61	15.3	10.26	9.93	15.38	5.06	5.31
	60	1.89	1.76	1.18	0.63	0.59	0.51	0.62	0.62	0.56
	40	1.10	1.16	0.34	0.36	0.35	0.32	0.35	0.38	0.31
	20	0.58	0.41	0.21	0.21	0.20	0.21	0.23	0.19	0.17
CLSUnSAL	240 (Full)	47.32	46.72	47.12	46.96	46.91	47.68	47.08	46.77	47.46
	60	12.83	13.19	12.84	12.90	13.52	13.02	12.77	12.99	13.04
	40	10.85	10.60	10.73	10.68	10.67	10.75	10.97	10.81	10.77
	20	8.50	8.64	8.66	8.81	8.65	8.67	8.73	9.34	8.72
Spectral library: $\mathbf{A}_2$										
Method	Library size	DC4 ($k = 3$)			DC5 ($k = 6$)			DC6 ($k = 9$)		
		SNR=30dB	SNR=40dB	SNR=50dB	SNR=30dB	SNR=40dB	SNR=50dB	SNR=30dB	SNR=40dB	SNR=50dB
NCLS	240 (Full)	9.01	8.63	8.64	8.87	9.56	9.83	10.35	8.43	8.44
	60	1.4	1.15	1.23	1.12	1.39	1.01	1.11	0.88	0.44
	40	0.8	0.86	0.81	0.84	0.70	0.51	0.83	0.89	0.29
	20	0.36	0.37	0.35	0.39	0.39	0.21	0.30	0.29	0.21
SUnSAL	240 (Full)	10.39	10.53	11.09	10.31	10.66	11.01	10.38	10.66	11.04
	60	1.85	1.67	1.57	1.57	1.67	1.13	1.60	1.36	0.68
	40	1.16	1.05	0.99	1.07	1.06	0.69	1.05	1.11	0.39
	20	0.55	0.65	0.59	0.58	0.66	0.17	0.62	0.42	0.38
CLSUnSAL	240 (Full)	32.71	32.95	32.67	32.93	33.07	32.91	32.77	33.13	32.94
	60	13.42	12.70	12.93	13.04	13.04	12.61	13.15	13.69	12.74
	40	10.43	10.65	10.42	10.31	10.11	10.39	10.28	10.12	10.41
	20	7.96	8.16	8.03	8.10	8.01	7.93	8.02	8.09	7.93

by measuring the reflectance of a number of pure soil, sunlit crown and weed spectra in each plot. Measurements were taken from nadir at 1 m above the object of interest. The relative cover of each material was extracted from digital images of a Sony DCP-P8/3.2-megapixel camera. This dataset has previously been used in [44] and has the advantage that true spectral endmembers and cover fraction distributions are available. For a more detailed description of the experimental set-up conducted in order to obtain the reference information for this scene, we refer to [44].

The spectral library used in our experiments, denoted by $\mathbf{B}$, is a collection of 971 spectra acquired on the ground in different days, including the day in which the data were acquired. The library comprises 85 soil spectra, 839 tree spectra and 57 weed spectra, with 1798 spectral bands in the spectral range from 350–2500 nm. From these set of spectra, 52 soil spectra, 76 tree spectra and 49 weed spectra were acquired the same day as the data were collected. Thus, these endmembers can be considered as the ones generating the observations. The algorithms detailed in section III were used to unmix the data using the full library and two pruned versions: $\mathbf{B}_1$ and $\mathbf{B}_2$, respectively containing subsets of 200 and 100 spectra from $\mathbf{B}$. In our experiments, we considered only the results computed *per group* as this strategy is the most appropriate bearing in mind the structure of the hyperspectral data and the available library. The threshold used in computing the probability of success is set to 10dB, and the data subspace was estimated using the HySime algorithm. This approach estimated the subspace dimension to be 56. Consequently, the first 56 eigenvectors returned by HySime were retained to define the estimated data subspace.

Fig. 7 shows the projection errors measured for the members in $\mathbf{B}$, obtained after applying the proposed pruning

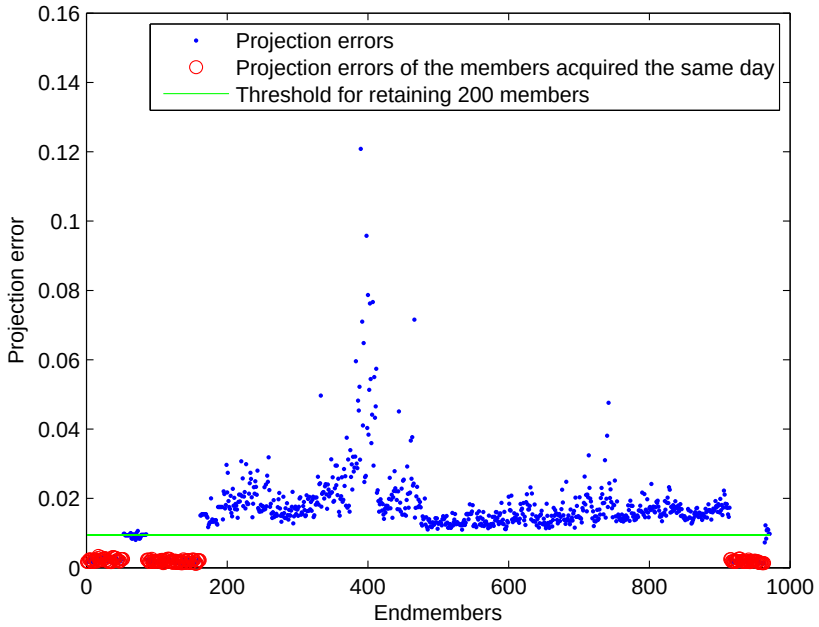

Fig. 7. Projection errors measured for the members in **B** in the experiment with real hyperspectral data, obtained after applying the proposed pruning methodology. The projection errors of the members acquired on the ground the same day as the hyperspectral data were collected are highlighted with red circles. The green line represents the threshold used when 200 members were retained from the library **B** in the pruning process.

methodology. The projection errors of the endmembers acquired on the ground the same day as the hyperspectral data were collected are highlighted with red circles. The green line represents the threshold used when 200 members were retained from the library $\mathbf{B}$ in the pruning process. Note that the members acquired at the same time as the image data always have projection errors close to zero. On the other hand, there is a clear gap between those members and all the other ones, which might help an end-user decide which signatures from the available library were the ones that really generate the considered hyperspectral data. Fig. 8 plots the best SRE(dB) scores obtained by the unmixing methods described in section III in each pixel of the considered dataset. The average SRE(dB), along with the probability of success p_s, are also indicated in the plots. In all cases, the regularization parameters involved in each method were tuned for optimal performance and only the best results from each considered unmixing method are reported. From Fig. 8, we conclude that the obtained unmixing performances always improve after dictionary pruning, an observation that was already emphasized in our experiments with simulated data. Note that, despite the fact that there are 177 spectra contained in the library that generates the data, the obtained results indicated that the unmixing accuracy computed per group still improves when only 100 members are retained. This is due to the fact that the retained endmembers can successfully explain the observed data without confusion resulting from the presence of supplementary members in the spectral library.

To conclude this section, Table VIII reports the computation times (in milliseconds) measured after applying

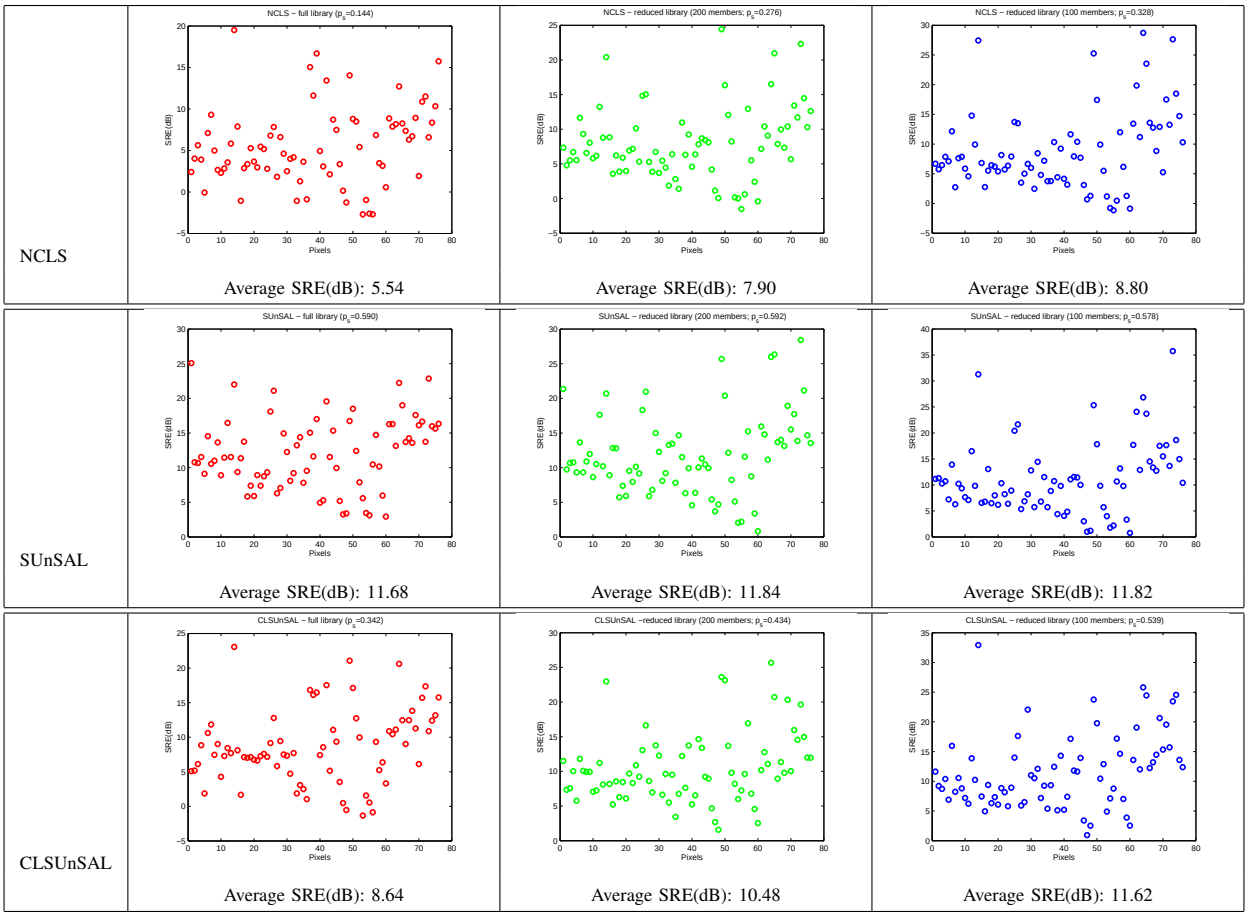

Fig. 8. The best SRE(dB) scores obtained by the considered unmixing methods in each pixel of the real hyperspectral dataset. The average SRE(dB), along with the probability of success p_s, are also indicated in the plotsT

the proposed unmixing algorithms to the real hyperspectral data set (with and without pruning) on a desktop PC with an Intel Core Duo CPU @2.5GHz and 4GB of RAM memory. The times reported in Table VIII correspond to the average running times, per pixel, for fixed values of the regularization parameters, where the parameters involved were optimized and set empirically to $\lambda = \lambda_C = 10^{-3}$. In all cases, the algorithms were set to run at most 1000 iterations. From Table VIII, we can conclude that the computing time of the considered algorithms decreases dramatically after the pruning is performed (the pruning time is always included in the times reported in Table VIII). A significant decrease in computation time is observed for unmixing methods which act per pixel (NCLS and SUnSAL). Combined with the experimental results with simulated data, the experiments conducted with real data indicate that the proposed dictionary pruning methodology is able to improve the unmixing accuracy and computational performance of the considered spectral unmixing algorithms.

VII. Conclusions and Future Work

In this paper, we have developed a new dictionary pruning methodology for spectral libraries intended to increase the accuracy of spectral unmixing algorithms while reducing their computation time. We exploit the fact

TABLE VIII

COMPUTATION TIMES (MILLISECONDS) FOR THE UNMIXING METHODS, WITH AND WITHOUT PRUNING, IN A REAL DATA EXPERIMENT

Method	$\mathbf{B}$ (971 members)	$\mathbf{B}_1$ (200 members)	$\mathbf{B}_2$ (100 members)
NCLS	24.20	1.47	0.80
SUnSAL	24.98	1.66	0.73
CLSUnSAL	125.65	32.08	20.32

that hyperspectral pixel vectors generally live in a lower-dimensional subspace. The proposed approach has been extensively evaluated using both real and hyperspectral data sets. In all cases, dictionary pruning reveals as a relatively simple yet very powerful strategy to improve unmixing performance, particularly when combined with sparse unmixing algorithms that conduct the estimation of fractional abundances using large spectral libraries, thus circumventing important problems such as the estimation of the number of endmembers (which translates here to the identification of an optimal subset of members in the considered spectral library) and the identification of the spectral signatures of such endmembers when there are no pure observations in the hyperspectral data. With the proposed pruning strategy, we bring sparse unmixing to a new domain in terms of computational performance (now much more manageable than in previous efforts such as [5], [9], [12]) and also in terms of unmixing performance, thus enhancing the practical application of sparse unmixing techniques in real problems. A possible direction for future work is to adapt the proposed pruning method to identify spectral signatures based on the physical parameters of the endmembers on the ground. Another research line worth being explored in future developments is how to exploit possible alternative ways of discriminating between actual states of the same endmembers in different scenarios (e.g., seasonal variations of the same endmember in different temporal periods).

VIII. ACKNOWLEDGEMENT

This work was supported by the European Communitys Marie Curie Research Training Networks Programme under contract MRTN-CT-2006-035927, Hyperspectral Imaging Network (HYPER-I-NET). Funding from the Spanish Ministry of Science and Innovation (CEOS-SPAIN project, reference AYA2011-29334-C02-02) and from the Portuguese Science and Technology Foundation, projects PEst-OE/EEI/LA0008/2011 and PTDC/EEA-TEL/104515/2008, is also gratefully acknowledged.

REFERENCES

[1] J. Adams, M. Smith, and P. Johnson, "Spectral mixture modeling: a new analysis of rock and soil types at the Viking Lander 1 site," *Journal of Geophysical Research*, vol. 91, pp. 8098–8112, 1986.

[2] D. Heinz and C.-I. Chang, "Fully constrained least squares linear mixture analysis for material quantification in hyperspectral imagery," *IEEE Transactions on Geoscience and Remote Sensing*, vol. 39, pp. 529–545, 2001.

[3] N. Keshava and J. Mustard, "Spectral unmixing," *IEEE Signal Processing Magazine*, vol. 19, no. 1, pp. 44–57, 2002.

[4] J. M. Bioucas-Dias, A. Plaza, N. Dobigeon, M. Parente, Q. Du, P. Gader, and J. Chanussot, "Hyperspectral unmixing overview: Geometrical, statistical and sparse regression-based approaches," *IEEE Journal of Selected Topics in Applied Earth Observations and Remote Sensing*, vol. 5, no. 2, pp. 354–379, 2011.

[5] D. Iordache, J. Bioucas-Dias, and A. Plaza, "Sparse unmixing of hyperspectral data," *IEEE Transactions on Geoscience and Remote Sensing*, vol. 49, no. 6, pp. 2014–2039, 2011.

[6] D. Iordache, "A sparse regression approach to hyperspectral unmixing," Ph.D. dissertation, Instituto Superior Tecnico, TULisbon, Lisbon, Portugal, 2011 (available online: http://www.lx.it.pt/ bioucas/files/PhD_Daniel_sparse_regression_2011.pdf).

[7] D. Donoho and M. Elad, "Optimal sparse representation in general (non-orthogonal) dictionaries via l1 minimization," *Proceedings of the National Academy of Sciences*, vol. 100, pp. 2197–2202, 2003.

[8] E. Candès, J. Romberg, and T. Tao, "Stable signal recovery from incomplete and inaccurate measurements," *Communications on Pure and Applied Mathematics*, vol. 59, no. 8, p. 1207, 2006.

[9] D. Iordache, J. M. Bioucas-Dias, and A. Plaza, "Total variation spatial regularization for sparse hyperspectral unmixing," *IEEE Transactions on Geoscience and Remote Sensing*, vol. 50, no. 11, pp. 4484–4502, 2012.

[10] D. Iordache, J. Bioucas-Dias, and A. Plaza, "Hyperspectral unmixing with Sparse Group Lasso," *IEEE International Geoscience and Remote Sensing Symposium IGARSS2011, Vancouver, Canada*, pp. 3586–3589.

[11] P. Sprechmann, I. Ramirez, G. Sapiro, and Y. Eldar, "C-Hilasso: a collaborative hierarchical sparse modeling framework," *IEEE Transactions om Signal Processing*, vol. 59, no. 9, pp. 4183–4198, 2011.

[12] D. Iordache, J. Bioucas-Dias, and A. Plaza, "Collaborative sparse regression for hyperspectral unmixing," *IEEE Transactions on Geoscience and Remote Sensing*, 2013 (accepted for publication, *in press*).

[13] J. M. Kim, O. K. Lee, and J. C. Ye, "Compressive music with optimized partial support for joint sparse recovery," *IEEE International Symposium on Information Theory (ISIT) Proceedings*, pp. 658–662, August 2011 (*arXiv:1102.3288v2*).

[14] ——, "Compressive music: A missing link between compressive sensing and array signal processing," *arXiv:1004.4398v5*, June 2011.

[15] Y. Eldar and H. Rauhut, "Average case analysis of multichannel sparse recovery using convex relaxation," *IEEE Transactions on Information Theory*, vol. 56, no. 1, pp. 505–519, 2010.

[16] J. Chen and X. Huo, "Theoretical results on sparse representations of multiple measurement vectors," *Mathematical Programming*, vol. 55, no. 12, p. 46344643, 2006.

[17] A. G. J. Tropp and M. Strauss, "Algorithms for simultaneous sparse approximation. Part I: Greedy pursuit," *Signal Processing*, vol. 86, no. 3, pp. 572–588, 2006.

[18] S. Cotter, B. Rao, K. Engan, and K. Kreutz-Delgado, "Sparse solutions to linear inverse problems with multiple measurement vectors," *IEEE Transactions on Signal Processing*, vol. 53, no. 7, pp. 2477–2488, 2005.

[19] D. Malioutov, M. Çetin, and A. Willsky, "A sparse signal reconstruction perspective for source localization with sensor arrays," *IEEE Transactions on Signal Processing*, vol. 53, no. 8, pp. 3010–3022, 2005.

[20] J. Tropp, "Algorithms for simultaneous sparse approximation. Part II: Convex relaxation," *Signal Processing*, vol. 86, no. 3, pp. 589–602, 2006.

[21] D. Wipf and B. Rao, "An empirical Bayesian strategy for solving the simultaneous sparse approximation problem," *IEEE Transactions on Signal Processing*, vol. 55, no. 7, pp. 3704–3716, 2007.

[22] M. Mishali and Y. Eldar, "Reduce and boost: Recovering arbitrary sets of jointly sparse vectors," *IEEE Transactions on Signal Processing*, vol. 56, no. 10, pp. 4692–4702, 2008.

[23] Y. Eldar, P. Kuppinger, and H. Bolcskei, "Block-sparse signals: Uncertainty relations and efficient recovery," *IEEE Transactions on Signal Processing*, vol. 58, no. 6, pp. 3042–3054, 2010.

[24] R. Baraniuk, V. Cevher, M. Duarte, and C. Hegde, "Model-based compressive sensing," *IEEE Transactions on Information Theory*, vol. 56, no. 4, pp. 1982–2001, 2010.

[25] R. Schmidt, "Multiple emitter location and signal parameter estimation," *IEEE Transactions on Antennas and Propagation*, vol. 34, no. 3, pp. 276–280, 1986.

[26] G. Bienvenu and L. Kopp, "Adaptivity to background noise spatial coherence for high resolution passive methods," in *IEEE International Conference on Acoustics, Speech, and Signal Processing, ICASSP'80.*, vol. 5. IEEE, 1980, pp. 307–310.

[27] P. Stoica and N. Arye, "MUSIC, maximum likelihood, and Cramer-Rao bound," *IEEE Transactions on Acoustics, Speech and Signal Processing*, vol. 37, no. 5, pp. 720–741, 1989.

[28] H. Krim and M. Viberg, "Two decades of array signal processing research: the parametric approach," *IEEE Signal Processing Magazine*, vol. 13, no. 4, pp. 67–94, 1996.

[29] J. Nascimento and J. Bioucas-Dias, "Hyperspectral subspace identification," *IEEE Transactions on Geoscience and Remote Sensing*, vol. 46, no. 10, pp. 2435–2445, 2008.

[30] M. Davies and Y. Eldar, "Rank awareness in joint sparse recovery," *IEEE Transactions on Information Theory*, vol. 58, no. 2, pp. 1135–1146, 2012.

[31] M. Pesavento and A. Gershman, "Maximum-likelihood direction-of-arrival estimation in the presence of unknown nonuniform noise," *IEEE Transactions on Signal Processing*, vol. 49, no. 7, pp. 1310–1324, 2001.

[32] M. Li and Y. Lu, "Maximum likelihood DOA estimation in unknown colored noise fields," *IEEE Transactions on Aerospace and Electronic Systems*, vol. 44, no. 3, pp. 1079–1090, 2008.

[33] R. Roger and J. Arnold, "Reliably estimating the noise in AVIRIS hyperspectral imagers," *International Journal of Remore Sensing*, vol. 17, no. 10, pp. 1951–1962, 1962.

[34] M. Mishali and Y. Eldar, "Reduce and boost: Recovering arbitrary sets of jointly sparse vectors," *IEEE Transactions on Signal Processing*, vol. 56, no. 10, pp. 4692–4702, October 2008.

[35] B. Turlach, W. Venables, and S. Wright, "Simultaneous variable selection," *Technometrics*, vol. 27, pp. 349–363, 2004.

[36] J. Bioucas-Dias and M. Figueiredo, "Alternating direction algorithms for constrained sparse regression: application to hyperspectral unmixing," *2nd Workshop on Hyperspectral Image and Signal Processing: Evolution in Remote Sensing (WHISPERS)*, pp. 1–4, 2010.

[37] M. Afonso, J. Bioucas-Dias, and M. Figueiredo, "An augmented Lagrangian approach to the constrained optimization formulation of imaging inverse problems," *IEEE Transactions on Image Processing*, vol. 20, no. 3, pp. 681 –695, 2011.

[38] J. Eckstein and D. Bertsekas, "On the Douglas-Rachford splitting method and the proximal point algorithm for maximal monotone operators," *Mathematical Programming*, vol. 5, pp. 293–318, 1992.

[39] J. Stuckens, S. Dzikiti, W. Verstraeten, S. Verreynne, R. Swennen, and P. Coppin, "Physiological interpretation of a hyperspectral time series in a citrus orchard," *Agricultural and Forest Meteorology*, vol. 151, no. 7, pp. 1002–1015, July 2011.

[40] J. Nascimento and J. Bioucas-Dias, "Vertex component analysis: a fast algorithm to unmix hyperspectral data," *IEEE Transactions on Geoscience and Remote Sensing*, vol. 43, no. 4, pp. 898–910, 2005.

[41] M. Zortea and A. Plaza, "Spatial preprocessing for endmember extraction," *IEEE Transactions on Geoscience and Remote Sensing*, vol. 47, pp. 2679–2693, 2009.

[42] M. Schaepman, S. Ustin, A. Plaza, T. Painter, J. Verrelst, and S. Liang, "Earth system science related imaging spectroscopy – an assessment," *Remote Sensing of Environment*, vol. 113, pp. 123–137, 2009.

[43] D. Iordache, J. Bioucas-Dias, and A. Plaza, "Dictionary pruning in sparse unmixing of hyperspectral data," *4th IEEE GRSS Workshop on Hyperspectral Image and Signal Processing: Evolution in Remote Sensing (WHISPERS), Shanghai, China*, pp. 1–4, 2012.

[44] B. Somers, K. Cools, S. Delalieux, J. Stuckens, D. V. der Zande, W. Verstraeten, and P. Coppin, "Nonlinear hyperspectral mixture analysis for tree cover estimates in orchards," *Remote Sensing of Environment*, vol. 113, no. 6, pp. 1183–1193, June 2009.